Imogolite: an aluminosilicate nanotube endowed with low cytotoxicity and genotoxicity

Chemical Research in Toxicology

Article

pubs.acs.org/crt

Imogolite: An Aluminosilicate Nanotube Endowed with Low Cytotoxicity and Genotoxicity

Bianca Maria Rotoli,[†,∇] Patrizia Guidi,[§,∇] Barbara Bonelli,[∥,∇] Margherita Bernardeschi,[§] Massimiliano G. Bianchi,[‡] Serena Esposito,[⊥] Giada Frenzilli,[§] Paolo Lucchesi,[§] Marco Nigro,[§] Vittoria Scarcelli,[§] Maura Tomatis,[#] Pier Paolo Zanello,[†] Bice Fubini,[*,#] Ovidio Bussolati,[*,†] and Enrico Bergamaschi[‡]

[†]Department of Biomedical, Biotechnological and Translational Sciences (SBiBiT) and [‡]Department of Clinical and Experimental Medicine, University of Parma, 43125 Parma, Italy

[§]Department of Clinical and Experimental Medicine, University of Pisa, 56126 Pisa, Italy

[∥]Department of Applied Science and Technology and INSTM, Unit of Torino Politecnico, Politecnico di Torino, 10129 Turin, Italy

[⊥]Department of Civil and Mechanical Engineering, University of Cassino and Southern Lazio, 03043 Cassino, Italy

[#]Department of Chemistry and "G. Scansetti" Interdepartmental Center for Studies on Asbestos and Other Toxic Particulates, University of Torino, 10125 Turin, Italy

ABSTRACT: High-aspect-ratio nanomaterials (HARN) (typically, single-walled carbon nanotubes (SWCNT) or multiwalled carbon nanotubes (MWCNT)) impair airway barrier function and are toxic to macrophages. Here, we assess the biological effects of nanotubes of imogolite (INT), a hydrated aluminosilicate $[(OH)_3Al_2O_3SiOH]$ occurring as single-walled NT, on murine macrophages and human airway epithelial cells. Cell viability was assessed with resazurin. RT-PCR was used to study the expression of *Nos2* and *Arg1*, markers of classical or alternative macrophage activation, respectively, and nitrite concentration in the medium was determined to assess NO production. Epithelial barrier integrity was evaluated from the trans-epithelial electrical resistance (TEER). Potential genotoxicity of INT was assessed with comet and cytokinesis-block micronucleus cytome assays. Compared to MWCNT and SWCNT, INT caused much smaller effects on RAW264.7 and MH-S macrophage viability. The incubation of macrophages with INT at doses as high as 120 $\mu g/cm^2$ for 72 h did not alter either *Nos2* or *Arg1* expression nor did it increase NO production, whereas IL6 was induced in RAW264.7 cells but not in MH-S cells. INT did not show any genotoxic effect in RAW264.7 and A549 cells except for a decrease in DNA integrity observed in epithelial A549 cells after treatment with the highest dose (80 $\mu g/cm^2$). No significant change in permeability was recorded in Calu-3 epithelial cell monolayers exposed to INT, whereas comparable doses of both SWCNT and MWCNT lowered TEER. Thus, in spite of their fibrous nature, INT appear not to be markedly toxic for *in vitro* models of lung−blood barrier cells.

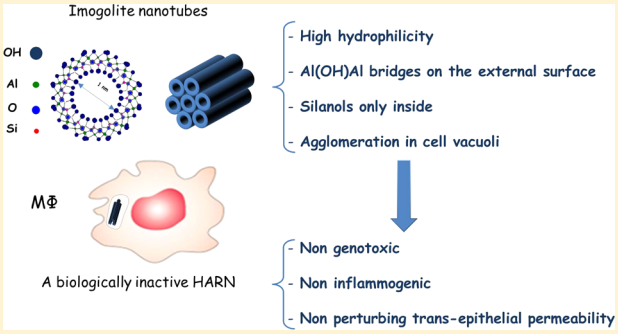

INTRODUCTION

Different kinds of nanomaterials are increasingly being produced for different technical and biomedical applications because of their peculiar mechanical and electrical properties. However, the consequences of the interaction of these novel materials with biological systems are often not completely understood, and their potentially toxic effects are still the object of debate and a cause for concern.[1−4]

Among nanomaterials, carbon nanotubes (CNT) and other high-aspect-ratio nanomaterials (HARN) cause concern because of their asbestos-like morphology. Evidence exists demonstrating that a fraction of CNT reaches the pleura, with consequent retention of long fibers, inflammation, fibrosis, and several pathologies, including mesothelioma, similar to that observed for asbestos fibers.[5] The question arises as to whether any nanotube with a close morphology would exert the same effect or whether different materials might behave in quite different ways.[6,7]

Imogolite is a nanotubular aluminosilicate with $(OH)_3Al_2O_3SiOH$ stoichiometry that naturally occurs in volcanic soils and may be also obtained with high purity by sol−gel synthesis.[8,9] Imogolite nanotubes (INT) exhibit Al−O−Al and Al(OH)Al groups at the outer surface and SiOH groups at the inner surface, as shown in Scheme 1. Typically, INT have an inner diameter of about 1.0 nm, an outer diameter of 2.0−2.7 nm, and variable length in the micrometer range;[10] thus, they structurally resemble single-walled carbon nanotubes (SWCNT).

Received: January 2, 2014
Published: June 3, 2014

   dx.doi.org/10.1021/tx500002d | *Chem. Res. Toxicol.* 2014, 27, 1142−1154

Scheme 1. Cross-Section of an Imogolite Nanotube Showing Its Chemical Composition[a]

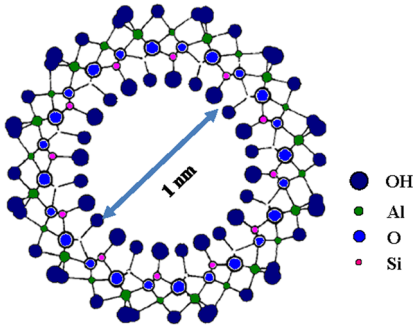

[a]The inner diameter is about 1.0 nm.

Once formed, INT are expected to arrange as a porous network of interwoven bundles with three kinds of pores, depicted in Scheme 2,[11] (A) intratube nanopores (about 1 nm wide), (B) intertube pores corresponding to the spacing among three aligned nanotubes in a regular packing (0.3−0.4 nm wide), and (C) slit mesopores among bundles.

Scheme 2. Bundles of INT[a]

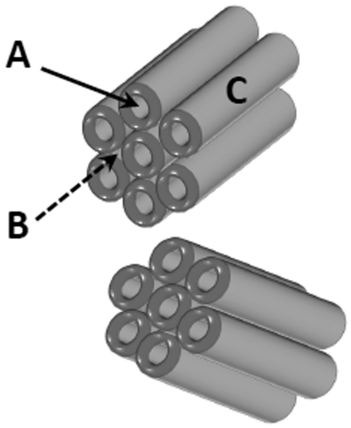

[a](A) Intratube pores, (B) intertubes pores, and (C) slit mesopores among bundles.

Besides being a subject of interest in the pedological field, INT are endowed with properties[12−14] that render them candidates for several industrial applications, such as separation or storage of gas,[14−16] uptake of anions and cations from water,[17,18] and catalysis.[9,19] This variety of potential applications explains the interest in synthesizing imogolite-like structures, such as single- or double-walled aluminogermanate nanotubes.[20−24]

Very little information is available on INT toxicity. A study concerning an aluminogermanate imogolite analogue reports length- and dose-dependent genotoxic effects in the absence of significant cytotoxic events in cultured human fibroblasts.[25] However, it must be noted that, besides their different chemical composition, aluminogermanate NT are shorter in length and have a larger diameter, thereby exhibiting a markedly different morphology than that of proper INT. Because INT can be synthesized and aligned into densely packed arrays oriented in a single dimension,[26] they may be of interest as a biological scaffold that mimics the fibrous morphology of type I collagen. Indeed, a single study on the possible biomedical applications of INT[26] shows that they have good biocompatibility in osteoblast cultures in terms of cell spreading, cell proliferation, and enhanced matrix mineralization; however, possible toxicity has not been investigated.

The present study has been undertaken to assess INT biological effects *in vitro* using macrophages and airway epithelial cells, two cell models in which HARN toxicity has been repeatedly investigated. For this purpose, INT with controlled morphology have been synthesized and employed in several toxicity-related tests. Physicochemical characterization has included material morphology, surface charge, specific surface area, and hydrophilicity. In order to assess a large number of properties usually associated with lung damage, the ability to generate free radical species in a cell-free test as well as cellular uptake, cell viability, genotoxicity, macrophage activation, and changes in epithelial permeability have been investigated.

EXPERIMENTAL PROCEDURES

Materials. Imogolite nanotubes (INT) were synthesized according to a method described previously:[9,27] at 20 °C, TEOS (tetraethoxysilane) and Al(*s*-butoxide)$_3$ were added to a 75 mM aqueous solution of $HClO_4$ in a Si/Al/$HClO_4$ molar ratio of 1:2:1. A slight excess of TEOS was used in order to prevent preferential formation of aluminum hydroxide during hydrolysis. The solution was stirred for 18 h, diluted to 20 mM in Al, autoclaved at 100 °C for 4 days, dialyzed for 4 days against deionized water, and then dried at 50 °C.

Commercial SWCNT (Aldrich 636797, lot 12526AE, 1.1 nm × 5−15 μm, BET 400 m^2/g, according to the manufacturer) were also obtained from Sigma-Aldrich. They consist of SWCNT (>50%) and of other nanotubes (MWCNT and double-walled CNT, 40%) with <5% amorphous carbon and traces of metals (Co, 0.6%; Mg, 1.2%; and Mo, 0.1%), as declared by the supplier. Commercial MWCNT (Aldrich 659258, 110−170 nm × 5−9 μm) were obtained from Sigma-Aldrich, Milan, Italy. MWCNT (Aldrich 659258) have a specific surface area (SSA) of 22.6 ± 0.38 m^2/g and are largely made of multiwalled nanotubes (at least 90%), with residual amorphous carbon and metal traces (iron, <0.1%; as declared by the supplier).

Characterization of Imogolite Nanotubes. Field-emission scanning microscopy (FE-SEM) images of the three nanomaterials were collected with a high-resolution FE-SEM instrument (LEO 1525) equipped with a Gemini field-emission column.

SSA was measured according to the BET (Brunauer−Emmett−Teller) method. N_2 adsorption isotherms were measured at −196 °C on INT previously outgassed at 300 °C in order to remove water and other atmospheric contaminants while still preserving INT integrity (Quantachrome Autosorb 1C instrument). Nonlocal density functional theory (NL-DFT)[28] was used to evaluate pore size distribution (PSD) by applying a N_2-silica kernel.

The surface electrical charge of INT was evaluated by their ζ-potential in water, in two complete cell culture media, namely, F12 and MEM, supplemented with 10% fetal bovine serum (FBS), and in the same media without FBS. Electrophoretic mobility as a function of pH was measured at 25 °C by means of electrophoretic light scattering (ELS) on a Zetasizer Nano-ZS (Malvern Instruments, Worcestershire, UK). The corresponding ζ-potential curves were calculated according to Henry's equation: $U_E = 2\varepsilon\zeta f(K_a)/3\eta$, where U_E is the electrophoretic mobility, ε is the dielectric constant, ζ is the zeta potential, $f(K_a)$ is Henry's function, and η is the viscosity. The adopted value of $f(K_a)$ was 1.5 according to Smoluchowski's approximation, which is usually applied to aqueous solutions of moderate electrolyte concentration, like those in the present case. The ζ-potential values determined in this manner did not differ much from those obtained by more sophisticated models.[29] INT suspensions were obtained after 2 min of sonication with an ultrasonic probe (100 W, 20 kHz, Sonoplus; Bandelin, Berlin, Germany); the pH of the suspension was adjusted by adding either 0.1 M HCl or 0.1 M NaOH.

Surface hydrophilicity was evaluated by gas−solid adsorption microcalorimetry. A heat flow microcalorimeter (Calvet-type, Setaram, France) connected to a high-vacuum gas volumetric glass apparatus was

dx.doi.org/10.1021/tx500002d | *Chem. Res. Toxicol.* 2014, 27, 1142−1154

employed. Subsequent doses of water vapor were admitted onto the sample, and adsorbed amounts, released heat, and equilibrium pressure were measured for each dose when the thermodynamic equilibrium was attained. The calorimeter was maintained at 30 °C throughout the adsorption experiment. The equilibrium pressure (p_{H_2O}, Torr) was monitored by means of a transducer gauge (Barocell 0−100 Torr, Edwards). A typical adsorption sequence comprised three subsequent runs using the following procedure: (i) dosing successive amounts of water vapor onto the sample up to a defined equilibrium pressure, typically 10 Torr (Ads I), (ii) desorption at 30 °C under vacuum, and (iii) readsorption of similar doses up to the same pressure in order to evaluate the fraction of adsorbate that is reversibly held at the surface (Ads II). Adsorbed amounts were normalized to the unit surface area (n_{ads}, micromoles per square meter) and plotted in the form of volumetric isotherms. Differential heats of adsorption, which represent the enthalpy changes ($q^{diff} = -\Delta_{ads}H$) associated with the process, were plotted as a function of the increasing water uptake. Prior to the adsorption measurement, the sample was outgassed in the calorimetric cell for 2 h at 150 °C and subsequently transferred into the calorimetric vessel without any exposure to the atmosphere.

Free Radical Generation in a Cell-Free Test. Free radical release upon incubation of INT with either H_2O_2 (yielding hydroxyl radicals) or sodium formate (yielding carbon centered radicals as a consequence of homolytic cleavage of a C−H bond) was measured by electron paramagnetic resonance (EPR) spectroscopy using the spin trapping technique with 5,5′-dimethyl-1-pyrroline-*N*-oxide (DMPO) as the trapping agent according to a procedure that is well-established in our laboratory.[30] Two amounts (7 and 70 mg) of powder were tested. HO$^{\bullet}$ generation was measured by suspending INT in 500 μL of 0.5 M phosphate buffer (pH 7.4) and then adding 250 μL of 0.17 M DMPO and 500 μL of 0.2 M H_2O_2. The production of $CO_2^{\bullet-}$ radicals was measured by suspending INT in 500 μL of 0.17 M DMPO and then adding 500 μL of a 2 M sodium formate solution in 0.5 M phosphate buffer. The number of radicals released is proportional to the intensity of the EPR signal measured by double integration. Kinetics of free radical yield was followed for at least 1 h.

Cell Culture and Treatments. For viability and gene expression studies, two murine macrophage cell lines were used: RAW264.7, obtained from the Istituto Zooprofilattico Sperimentale della Lombardia (Brescia, Italy) and MH-S,[31] obtained from Prof. Dario Ghigo, Department of Biochemistry, University of Turin. Cells were cultured in RPMI. These lines have been extensively used in toxicological studies.[32−36]

For genotoxicity studies, RAW264.7 cells, cultured in minimal essential medium (MEM), and alveolar carcinoma A549 cells, cultured in F-12 medium, were provided by Prof. Lucia Migliore, University of Pisa. RAW264.7 and A549 cells were selected because they are widely used to assess genotoxicity effects of nanomaterials *in vitro*.[37,38]

For studies of epithelial permeability, Calu-3 cells, derived from a human lung adenocarcinoma,[39] were obtained from the Istituto Zooprofilattico Sperimentale della Lombardia (Brescia, Italy) and cultured in Eagle's minimum essential medium (EMEM) supplemented with 1 mM sodium pyruvate. Calu-3 cells have been extensively used in recent studies to investigate airway epithelium permeability.[40−46]

For all cell types, media were supplemented with 10% FBS, 1% pen/strep, and 2 mM L-glutamine, and cultures were maintained at 37 °C under a humidified atmosphere of 5% CO_2/95% air.

Before the experiments, INT, SWCNT, and MWCNT were heated at 220 °C for 3 h to eliminate possible contamination from lipopolysaccharide (LPS). For viability and gene expression experiments, after cooling at room temperature, nanomaterials were dispersed at a concentration of 1 mg/mL in sterile phosphate-buffered saline (PBS) to obtain stock suspensions for a series of experiments. Immediately before each experiment, the materials were extensively vortexed, sonicated three times for 15 min in a Bransonic Ultrasound bath, and then added to normal growth medium to reach the desired concentration. No detergent was used to improve the solubility of nanomaterials in aqueous solutions. After the addition, CNT and INT tend to precipitate and form more or less expanded agglomerates, clearly detectable with optical microscopy, that come into contact with the cell monolayer (not shown). For genotoxicity studies, the highest dose was obtained by dispersing the nanotubes in the medium and obtaining the other doses by dilution in the wells.

Nominal doses were expressed as micrograms of nanotubes per square centimeter of monolayer.

Viability. Cell viability of RAW264.7 and MH-S was tested with the resazurin method[47] in cells seeded in 96-well dishes (30×10^3 cells/well). According to this method, viable cells reduce the nonfluorescent compound, resazurin, into the fluorescent compound, resorufin, which accumulates in the medium. After exposure to INT or CNT, carried on in thermostat, cells were incubated for 1 h with fresh, serum-free medium supplemented with 44 μM resazurin; fluorescence was then measured at 572 nm with a fluorimeter (Wallac 1420 Victor2Multilabel Counter, PerkinElmer).

For Calu-3 monolayers grown in a double-chamber culture system (see below), resazurin was added at both sides of the monolayer, and fluorescence was measured in the apical compartment.[48]

The possible interference of the nanomaterials with resazurin was assessed both in the absence and presence of cells. Although MWCNT and INT (both at a dose of 80 μg/cm^2 of culture surface) did not appreciably quench resorufin fluorescence, SWCNT produce significant dose-dependent quenching (data not shown). Therefore, the data on viability relative to treatment with SWCNT were adequately corrected, taking into account the contribution of quenching, through the empirical, experimentally derived formula $F_C = F_M \times (1 + 0.0083 \times D_S)$, where F_C is the corrected fluorescence, F_M is the measured fluorescence, D_S is the dose of SWCNT (expressed as micrograms per square centimeter).

Gene Expression. Total RNA, extracted from cells seeded in 6-well dishes (300×10^3 cells/well) that were grown to subconfluence with an RNeasy Mini Kit (Qiagen S.p.a., Milano, Italy), was reverse-transcribed, and 40 ng of cDNA was amplified and treated as described previously.[49] The forward and reverse primers (5 pmol each) that were used are detailed in Table 1. Quantitative PCR was performed in a 36-well Rotor

Table 1. Primers Used for RT-PCR Studies

gene	forward	reverse
Arg1	5′ CAG AAG AAT GGA AGA GTC AG 3′	5′ GGA GTG TTG ATG TCA GTG TG 3′
Nos2	5′ GTT CTC AGC CCA ACA ATA CAA GA 3′	5′ GTG GAC GGG TCG ATG TCA C 3′
Il6	5′ TAG TCC TTC CTA CCC CAA TTT CC 3′	5′ TTG GTC CTT AGC CAC TCC TTC 3′
Gapdh	5′ TGT TCC TAC CCC CAA TGT GT 3′	5′ GGT CCT CAG TGT AGC CCA AG 3′

Gene 3000, version 5.0.60 (Corbett Research, Mortlake, Australia). Fluorescence was monitored at the end of each extension step. A no template, no reverse transcriptase control was included in each experiment. At the end of the amplification cycles, melting curve analysis was added. RT-PCR data are expressed as the ratio between the mRNA of interest and that of *Gapdh*.

Nitric Oxide Production. The production of NO was assessed through the quantification of nitrites, stable derivatives of NO, in the culture medium by employing a fluorimetric approach described previously.[50] Nitrite concentration was calculated from a calibration curve performed with $NaNO_2$ standards and expressed in nanomoles per milliliter of extracellular medium (micromolar). Calibration curves, performed in the absence or presence of INT at a dose of 120 μg/cm^2 of culture surface, were comparable (data not shown), indicating that INT do not interfere with the method.

Comet Assay. RAW264.7 and A549 cells were seeded and treated for DNA damage evaluation as previously described.[38] Single-cell gel electrophoresis (or Comet assay) was performed according to Singh et al.[51] with slight modifications. Briefly, cell suspensions were embedded in agarose, spread onto microscope slides, lysed (NaCl 2.5 M, Na_2EDTA 100 mM, Trizma base 10 mM, 10% dimethyl sulfoxide, 1% Triton X-100, pH 10) and kept for at least 1 h at 4 °C in the dark. Successively,

slides were treated with alkali (NaOH 300 mM, Na_2EDTA 1 mM, pH >13) and electrophoresed for 20 min at 25 V and 300 mA. After the run was complete, slides were neutralized with Tris−HCl (0.4 M, pH 7.5), stained with ethidium bromide, and observed under a fluorescence microscope (400×). The percentage of DNA migrating toward the anode (tail DNA) was quantified by an image analyzer (Kinetic Imaging Ltd., Komet, Version 5). At least 25 nuclei per slide and two slides per sample were scored, and the average value was calculated. A total of 300 cells were scored for each experimental point. Three independent experiments were carried out for each treatment. Cell viability was assessed by the Trypan blue dye exclusion technique.

Cytokinesis-Block Micronucleus Cytome Assay. RAW264.7 and A549 cells were seeded and treated for cytogenetic studies as previously reported.[51] Cytochalasin B (4 μg/mL) was added 44 h after seeding. Cells were washed with Hanks' balanced salt solution 72 h after seeding, detached, and centrifuged at 500*g* for 10 min. Pellets were treated with 1 mL of hypotonic solution (KCl 0.075 M) at 37 °C and prefixed with methanol/acetic acid, 3:5. Cells were centrifuged, and pellets were suspended in a fresh, cold (4 °C) fixative solution (methanol/acetic acid, 7:1) and then kept at 4 °C for at least 30 min. After a second fixative step, cells were dropped onto slides and stained with 2% Giemsa. One thousand binucleated cells per slide were analyzed, and two slides for each well were set up, for a total of 4000 cells scored per treatment. Two independent experiments were carried out for each treatment. Micronuclei (MN) and nucleoplasmic bridges (NPB) were scored according to the criteria set by Fenech,[52,53] and their frequency was recorded as the percent of binucleated cells.

Trans-Epithelial Electrical Resistance. For measurements of the trans-epithelial electrical resistance (TEER), Calu-3 cells were seeded into double-chamber culture inserts on membrane filters (pore size of 0.4 μm) for use with Falcon 24-well multitrays (cat. no. 3095, Becton, Dickinson & Company, Franklin Lakes, NJ, USA) at a density of 75×10^3 cells/300 μL. Measurements of TEER were made on monolayers grown for 10−14 days using an epithelial voltohmeter (EVOM, World Precision Instruments Inc., Sarasota, FL, USA). Materials were added in the apical chamber from a 1 mg/mL stock solution without changing the medium. TEER changes were expressed as the percentage of the initial value adjusted for control cell layers according to the following equation:[54]

$$\Delta_{TEER}\ (\%) = \frac{\text{final TEER}_{treated}}{\text{final TEER}_{control}} \times \frac{\text{initial TEER}_{control}}{\text{initial TEER}_{treated}} \times 100$$

Internalization. To test INT internalization, cells exposed for 24 h to 80 μg/cm^2 of INT were centrifuged, washed, treated with Karnovsky fixative for 5 h at 36.4 °C, washed in 0.1 M sodium cacodylate solution overnight, postfixed in 1% osmium tetroxide for 2 h in the dark at room temperature, newly washed with the same buffer solution, and dehydrated in a graded series of ethanol. Samples were pre-embedded in epon-araldite−propylene oxide 1:1 mixture overnight followed by pure epon-araldite for 6 h and then embedded in epon-araldite at 60 °C for 48 h.[55] Ultrathin sections (70−90 nm) were cut using a Reichert−Jung Ultracut E ultramicrotome, collected on 200-mesh carbon-coated copper grids stained with uranyl acetate and lead citrate, and observed with a JEOL 100 SX transmission electron microscope.

Statistical Analysis. Values of viability, TEER, and nitrite production were analyzed with ANOVA using a posthoc Bonferroni test, and expression data were evaluated with a Student's *t* test for unpaired data.

Multifactor analysis of variance (MANOVA) was carried out on comet and cytome assay data, considering dose, experimental time, culture, cell type, and experiment as factors. The multiple range test (MRT) was performed in order to detect differences among different experimental groups. Level of statistical significance was considered for p values < 0.05.

Reagents. L-Glutamine, FBS, and culture media were purchased from EuroClone SpA, Pero, Milan, Italy. Recombinant human interleukin-4 (IL-4) was obtained from RELIAThech GmbH, Wolfenbuttel, Germany. Sigma-Aldrich (Milan, Italy) was the source of all the other chemicals.

RESULTS

Characterization of Imogolite Nanotubes. Figure 1a shows a FE-SEM picture of imogolite nanotubes (INT). As reported in the literature and illustrated in Scheme 2, INT are several micrometers long and arranged into bundles that form an interwoven porous network so that it is not possible to observe single INT, only bundles.[9,14] No other morphology, such as spherical particles attributable to the presence of proto-imogolite, a common impurity in INT obtained by synthesis,[9] was observed by FE-SEM analysis, indicating that a pure INT sample was obtained. An image of SWCNT is reported in Figure 1b that confirms the presence of MWCNT in addition to actual SWCNT, as reported in the Experimental Procedures. The image of MWCNT shows the presence of large, 100−200 nm wide tubes (Figure 1c).

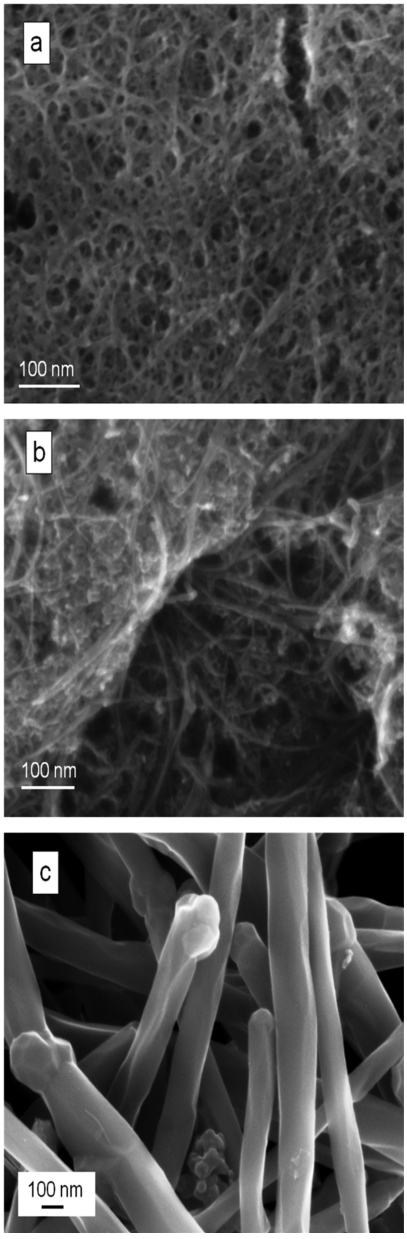

Figure 1. Selected FE-SEM micrographs of INT (a), SWCNT (b), and MWCNT (c).

dx.doi.org/10.1021/tx500002d | *Chem. Res. Toxicol.* 2014, 27, 1142−1154

Figure 2a reports the N_2 isotherm measured at −196 °C on dehydrated INT; a type I isotherm was observed, with no

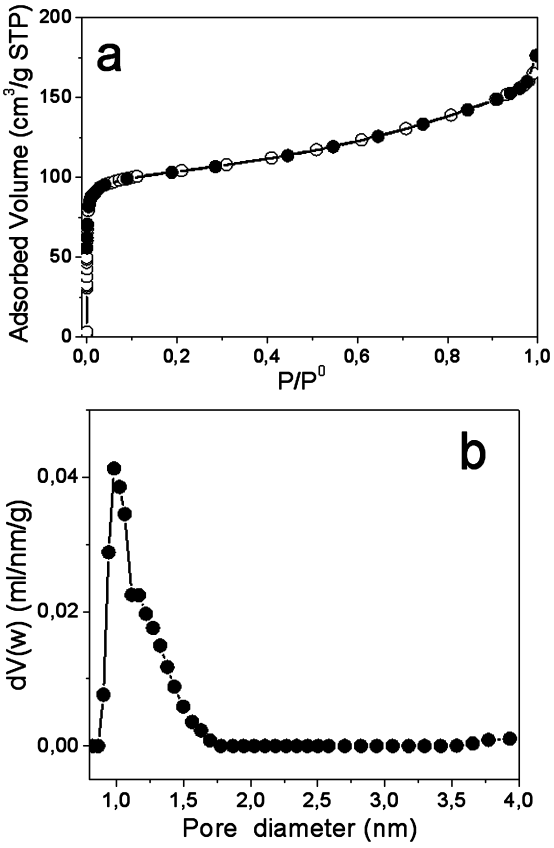

Figure 2. (a) N_2 isotherm at −196 °C on INT outgassed at 300 °C: black symbols, adsorption branch; white symbols, desorption branch. (b) PSD of INT outgassed at 300 °C obtained according to the NL-DFT method by applying a nitrogen-silica kernel to the adsorption branch of the isotherm.

hysteresis loop, as expected for INT.[9] The corresponding BET SSA was 384 m^2/g, and the overall microporous area (because of intratube pores) was indeed 261 m^2/g. Figure 2b reports the PSD obtained by applying the NL-DFT method to the isotherm adsorption branch: a major family of pores was seen with a maximum diameter of about 1.0 nm, assigned to intratube pores; larger (intertubes) pores are also present, in agreement with literature reports.[9]

ζ-Potentials of INT are reported in Figure 3. INT in water was positively charged at low pH, and the point of zero charge (PZC) was at pH 9.9, which is close to values reported in the literature for alumina particles.[56] This result is in agreement with the composition of the INT external surface, which exposes only Al−O−Al groups and Al(OH)Al bridges and should, therefore, behave as a hydrated aluminum oxide. According to the literature,[13] depending on the pH, the outer surface of INT may carry a positive net charge, whereas the inner surface would carry a corresponding negative net charge because of the following protonation equilibria:[17,18,57,58]

$$\mathrm{Al(OH)Al} + \mathrm{H^+} = \mathrm{Al(OH_2)^+Al} \quad (1)$$

$$\equiv\mathrm{SiOH} = \equiv\mathrm{SiO^-} + \mathrm{H^+} \quad (2)$$

The ζ-potential versus pH curve in water (solid circles) was markedly different from that measured in two cell culture media, F-12 (solid triangles) and MEM (solid squares) supplemented with FBS, in which very similar curves were obtained. The INT ζ-potential is lower when passing from pure water to the two cell culture media, with the PZC shifting to lower pH values (pH 4.2). Ions present in the two media may be adsorbed by INT, finally lowering the net charge, or, more likely, the loss of positive charges may be caused by adsorption of proteins from the serum present in the cell culture media. In order to clarify this point, measurements were run in the absence of FBS: similar curves were obtained with both F-12 (open triangles) and MEM (open squares), and PZC shifted to higher values. This result indicates a non-negligible role of bovine serum albumin (BSA), the major protein component of FBS, consistent with literature data that demonstrate BSA adsorption at the surface of alumina (Al_2O_3),[59] which has a similar composition to that of the INT external surface.

Surface hydrophilicity and distribution of strong sites for water adsorption were investigated by means of adsorption microcalorimetry following a technique established a long time ago that was previously employed for MWCNT[60] and amorphous silicas.[36,61] The adsorption isotherms of water vapor on INT preoutgassed at 150 °C are reported in Figure 4a, whereas the energy of interaction as a function of coverage is reported in Figure 4b. The initial heat was extremely high, suggesting the presence of surface sites able to strongly interact with water. The whole energy as a function of the coverage plot as well as uptake revealed an extremely high hydrophilicity that is opposite that of MWCNT, which are substantially hydrophobic.[60] The heat of interaction is even higher than what is usually found on silicas[36,61] and is close to the behavior of alumina,[62] which is in substantial agreement with the model described in Scheme 1 in which the external layer consists of aluminum octahedra.

Free Radical Generation. INT were tested for their potential in free radical release in the presence of either hydrogen peroxide (Fenton activity) or formiate ion (homolytic rupture of carbon−hydrogen bond) following a well-established procedure. Two doses (7 and 70 mg) were tested. In all cases, INT were fully inactive (data not shown), as opposed to what has been previously reported to take place on a large variety of toxic particles and fibers, including asbestos.[6,63]

Imogolite Nanotubes Are Less Toxic than Carbon Nanotubes on Macrophages. The effects of INT on cell viability, as assessed with the resazurin method, were compared with those of CNT (SWCNT and MWCNT), both known to exhibit marked cytotoxicity.[48,64] The effects of carbon nanotubes on murine macrophage (RAW264.7 and MH-S) viability are shown in Figure 5. A clear-cut dose-dependent toxicity was already evident for both SWCNT and MWCNT after 24 h of incubation, with a significant decrease in viability detected in either cell line at the minimal nominal dose used (10 $\mu g/cm^2$) and a viability loss of ≥80% detected at the maximal dose of 120 $\mu g/cm^2$. Under the same conditions, INT were completely ineffective up to 120 $\mu g/cm^2$ on MH-S cells, whereas only a modest 15% viability decrease was detected at 80 and 120 $\mu g/cm^2$ on RAW264.7 cells. Only for longer incubation periods did INT show significant effects on cell viability: up to a decrease of 35% at the maximal nominal dose (120 $\mu g/cm^2$) after 72 h of treatment. Under the same conditions, the viability of the two macrophage lines was completely suppressed by either SWCNT or MWCNT.

Imogolite Nanotubes Do Not Induce Markers of Classical or Alternative Macrophage Activation. The expression of activation markers in macrophages exposed to

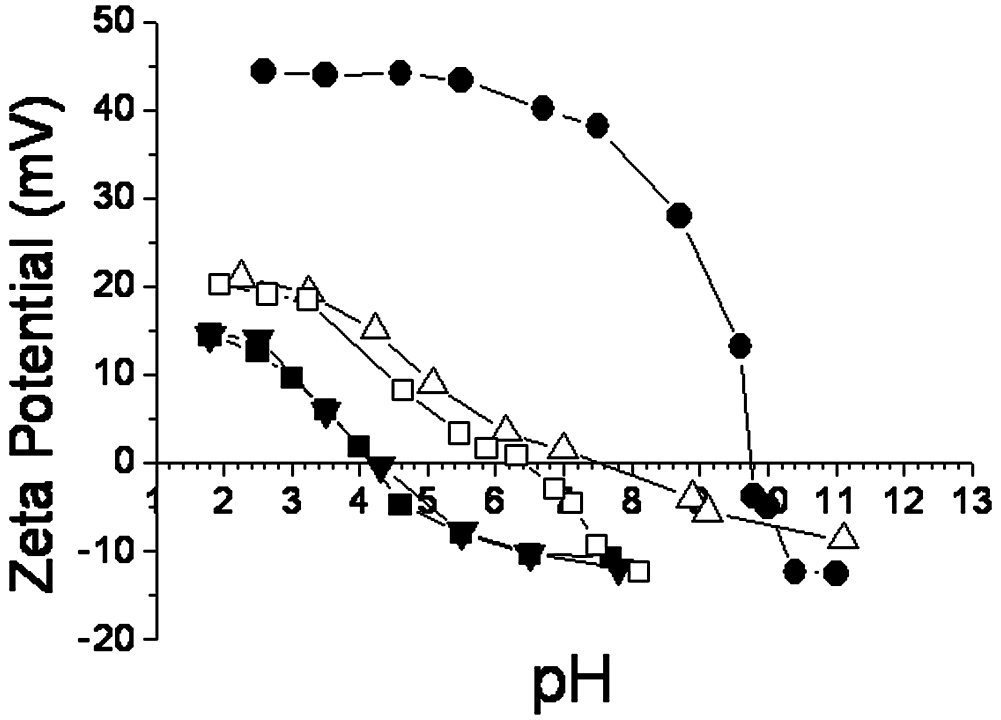

Figure 3. ζ-Potential curves of INT in water (black circles), F-12 medium (solid triangles), and MEM medium (solid squares), both supplemented with 10% FBS, and F-12 (open triangles) and MEM (open squares) in the absence of FBS.

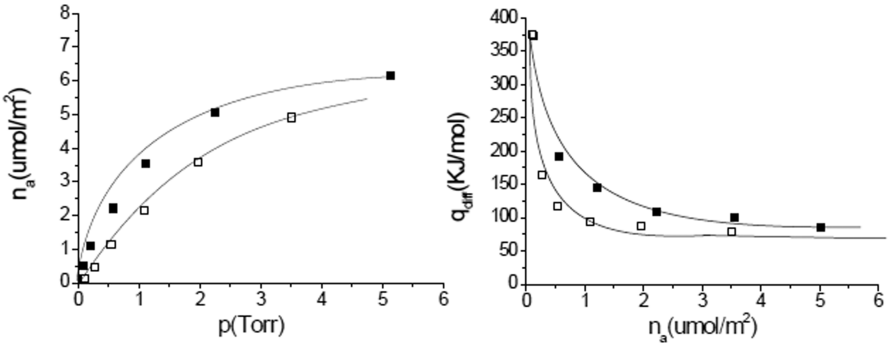

Figure 4. Adsorption of H_2O_{vap} at T = 30 °C on imogolite nanotubes outgassed 2 h at 150 °C. (a) Amount of water adsorbed as a function of the equilibrium pressure (n_{ads} vs p_{H_2O}). (b) Differential heat of adsorption as a function of the surface coverage (q_{diff} vs n_{ads}). Full symbols, total adsorption (Ads I); empty symbols, reversible adsorption (Ads II).

INT is shown in Figure 6. The gene for arginase 1 (*Arg1*), a typical marker of alternative activation,[65−68] was not induced by INT in both RAW264.7 and MH-S macrophages, whereas both cell types exhibited a clear *Arg1* induction when incubated with IL-4, used as a positive control (Figure 6a,d). The expression of *Nos2* for the inducible isoform of nitric-oxide synthase, a marker of classical macrophage activation,[69−71] was also not stimulated by INT, but it was increased by several-fold with the positive control, LPS (Figure 6b,e). The gene for interleukin-6 (*Il6*), a pro-inflammatory cytokine not specifically associated with either classical or alternative macrophage activation, was modestly induced by INT in RAW264.7 cells (Figure 6c) but not in MH-S macrophages, where a slight decrease was detected (Figure 6f).

The concentration of nitrites (as an indicator of NO production), determined in the extracellular medium of RAW264.7 cells incubated in the presence of INT, was not markedly different from that measured in control cells (Figure 7), consistent with the lack of *Nos2* induction observed under these conditions. On the contrary, nitrites were clearly accumulated in the extracellular medium of LPS-treated cultures. The nitrite concentration in the medium of LPS-treated cultures was comparable in the absence and presence of INT, indicating that imogolite did not affect the LPS-dependent *Nos2* induction.

Imogolite Nanotubes Do Not Exert Genotoxic Effects. INT did not exert any DNA damage at all of the doses and times investigated in RAW264.7 cells (Figure 8a), whereas a statistically significant increase in DNA damage was observed in A549 cells (Figure 8b) at 80 $\mu g/cm^2$ after 4 and 24 h exposures. However, under the same conditions and although no cytotoxicity was reported for RAW264.7 cells (Table 2), a significant increase in cell death was observed for A549 cells (Table 3). Therefore, it cannot be completely ruled out that DNA damage in epithelial cells was partially a consequence of cytotoxicity. CBMN-Cyt did not indicate any genotoxic effect after treatment with INT either in terms of MN frequency or of nucleoplasmic bridges in both of the cell lines used (Figure 9).

dx.doi.org/10.1021/tx500002d | *Chem. Res. Toxicol.* 2014, 27, 1142−1154

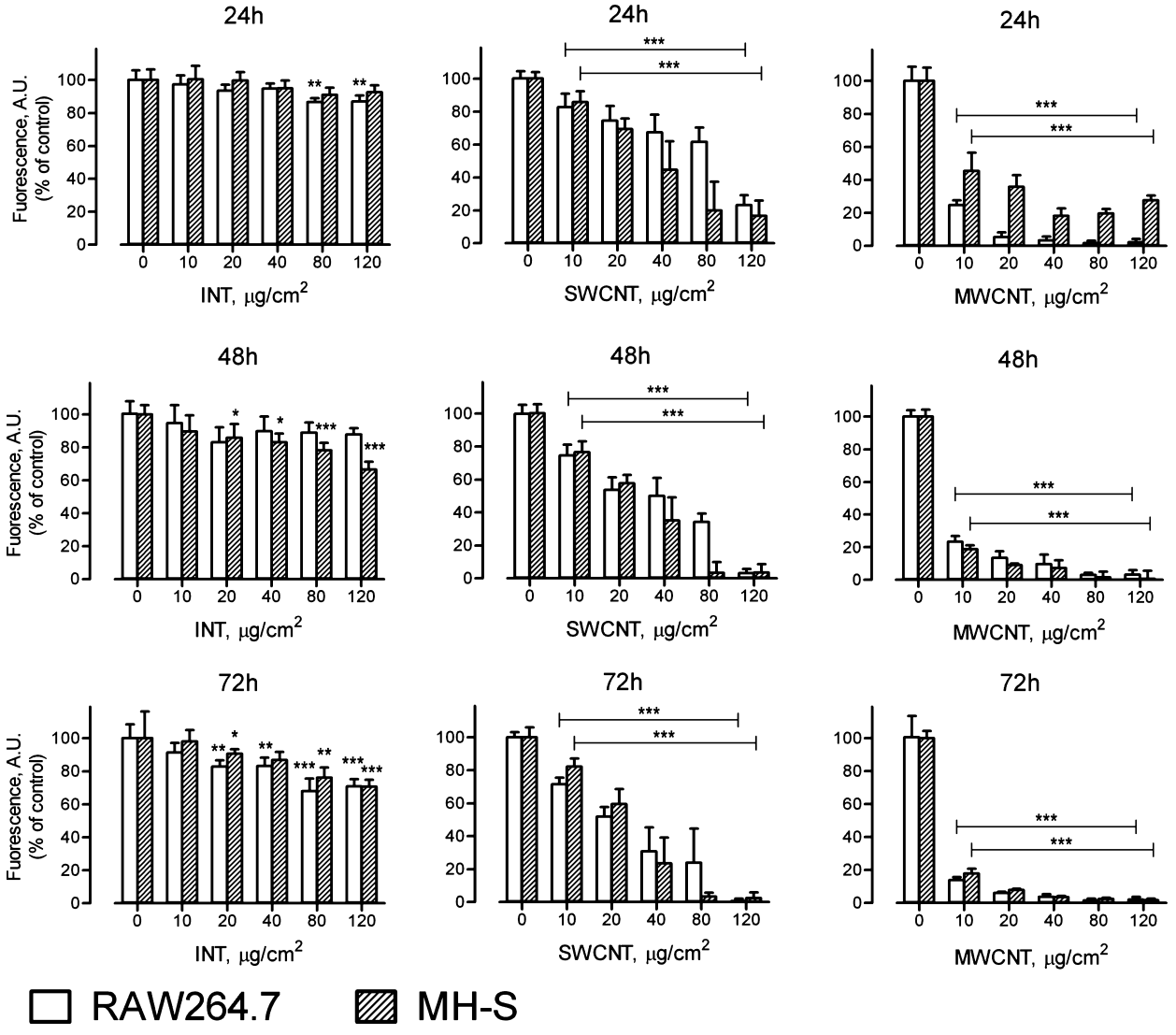

Figure 5. INT, SWCNT, and MWCNT effects on macrophage viability. Subconfluent cultures of RAW264.7 and MH-S murine macrophages, grown on 96-well dishes, were exposed for the indicated times to nominal doses of INT, SWCNT, and MWCNT ranging from 0 to 120 $\mu g/cm^2$, corresponding to 192 μg/mL. At the selected times, viability was assessed with the resazurin method. Data are the mean of five independent determinations with SD in a representative experiment performed four times with comparable results. * $p < 0.05$, ** $p < 0.01$, *** $p < 0.001$ vs control, untreated cultures.

Imogolite Nanotubes Are Internalized by Macrophages. TEM analysis showed the presence of dense inclusions composed of highly packed fibrous material assigned to INT in the cytoplasm of exposed RAW264.7 cells (Figure 10). Because of its high density, the fibrous material was often partly dislocated during ultrasectioning; however, it appeared to be compartmentalized within membrane-bound vacuoles (Figure 10a). Such inclusions were never observed in the cytoplasm of control cells (Figure 10b).

Imogolite Nanotubes Do Not Markedly Alter the Permeability of Airway Epithelial Cell Monolayers. A prolonged incubation with SWCNT or MWCNT progressively impairs the barrier properties of airway epithelial cells in a dose-dependent manner.[48,64] To compare the effects of carbon nanotubes and INT on the airway epithelial barrier, confluent monolayers of Calu-3 cells were incubated with the three types of nanotubes at a nominal dose of 80 $\mu g/cm^2$ of monolayer. TEER was measured after 7 days of treatment (Figure 11a). TEER was decreased by 50% in MWCNT-treated monolayers and by 40% in SWCNT-treated monolayers. On the contrary, INT did not alter TEER significantly, although the values were not significantly different from those measured in monolayers treated with SWCNT. Cell viability, evaluated with the resazurin method (Figure 11b) in the same monolayers, was not significantly affected by any kind of nanotube.

DISCUSSION

Recently, the interest in aluminosilicates in biological systems has been renewed by the finding that they can form intracellularly, at least in lower animals.[72] In these models, intracellular nanoparticles of aluminosilicates are considered to be nontoxic or even protective toward Al-mediated toxicity.[73] The biological effects of fibrous aluminosilicates are much less known, and the possibility of toxic effects related to their high aspect ratio has not been investigated in depth. The data reported in the present article clearly indicate that nanotubes of the aluminosilicate imogolite (INT) cause much milder cytotoxic effects than those of SWCNT and MWCNT on macrophages and airway epithelial cells.

dx.doi.org/10.1021/tx500002d | Chem. Res. Toxicol. 2014, 27, 1142−1154

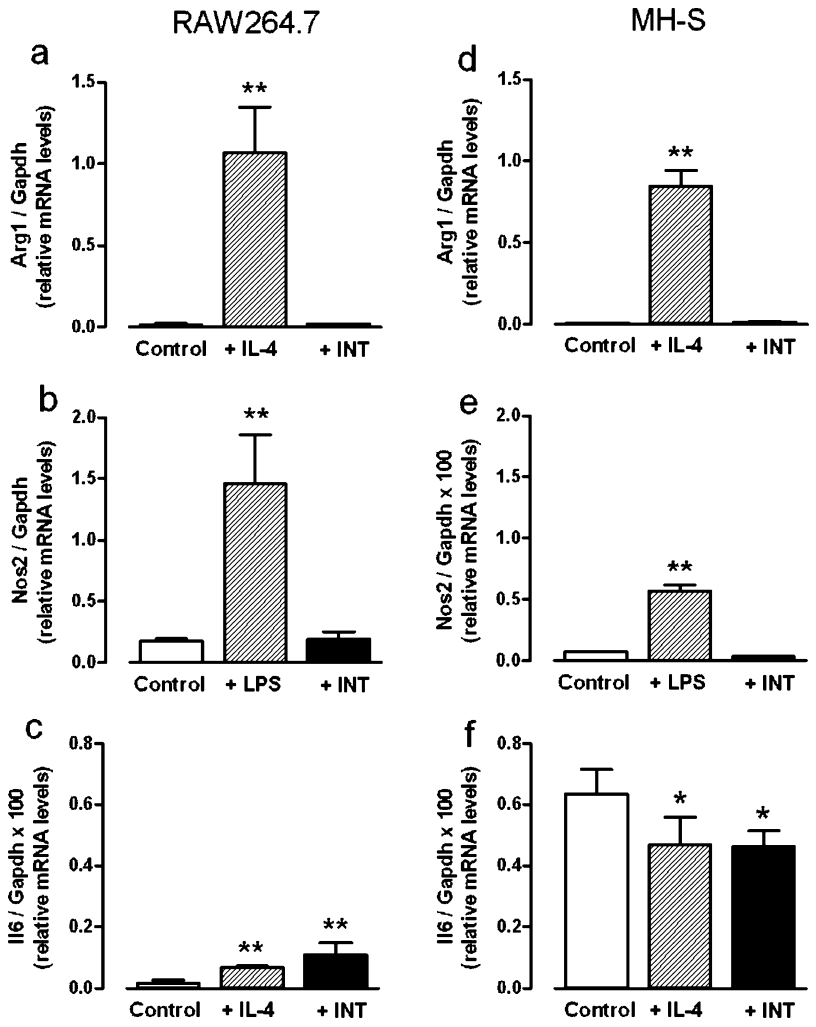

Figure 6. INT effects on gene expression in murine macrophages. RAW264.7 (a–c) or MH-S (d–f) cells were incubated in the presence of INT (120 μg/cm^2, 72 h), IL-4 (10 ng/mL, 24 h), or LPS (0.1 μg/mL, 18 h), as indicated. At the end of the treatment, mRNA was extracted, and the abundance of the mRNAs of *Arg1* (a, d), *Nos2* (b, e), and *Il6* (c, f) was determined and expressed vs the abundance of *Gapdh* mRNA. Data represent the mean of three independent determinations, each performed in duplicate (n = 3), with the SD shown. * $p < 0.05$, ** $p < 0.01$ vs control.

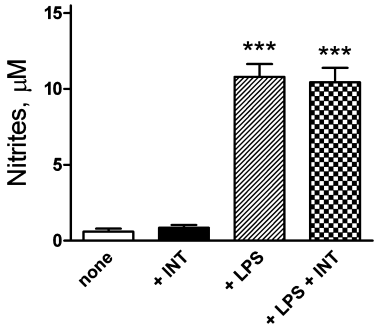

Figure 7. INT effects on nitrite concentration in the growth medium of murine macrophages. RAW264.7 cells were incubated in the presence of INT (120 μg/cm^2, 72 h), LPS (0.1 μg/mL, 18 h), or both, as indicated. The concentration of nitrites in the extracellular medium was determined at the end of the treatment. Data represent the mean of six independent determinations with the SD obtained in a representative experiment, which was performed two times with comparable results. *** $p < 0.001$ vs control.

In both of the macrophage models adopted, RAW264.7 and MH-S cells, INT exerted a very modest, although significant, dose- and time-dependent cytotoxicity; after a 72 h exposure, the IC_{50} was not reached at the maximal dose used of 120 μg/cm^2, and NOAEL was 10 μg/cm^2. Under the same exposure conditions, both MWCNT and SWCNT caused a substantial loss of viability. Moreover, although INT were internalized in the macrophages, no evidence of genotoxic effects was obtained with the comet and CBMN-Cyt assays in RAW264.7 cells. The lack of genotoxicity may be due to the fact that, as shown from the morphological evidence, INT are present as agglomerates in vacuoles and hence may be less able to reach intracellular sensitive targets, which is analogous to what has been described for MWCNT by Muller et al.[74] In addition, INT were not able to generate radical species under cell-free conditions. The absence of particle-derived free radicals is not surprising because aluminum is a simple trivalent cation incapable of redox changes, and no impurities (e.g., transition metal ions) were detected on the surface of INT.

These data appear to be partially different from those reported for imogolite-like aluminogermanate nanofibers on cultured human fibroblasts,[25] where weak cytotoxicity but dose-dependent DNA damage and increased micronucleated cell frequency were detected even at very low concentrations of the "small" fibers (5 to 6 nm).[25] Weaker genotoxicity was observed with long fibers. Differences in the cell model, exposure time, fiber

dx.doi.org/10.1021/tx500002d | *Chem. Res. Toxicol.* 2014, 27, 1142–1154

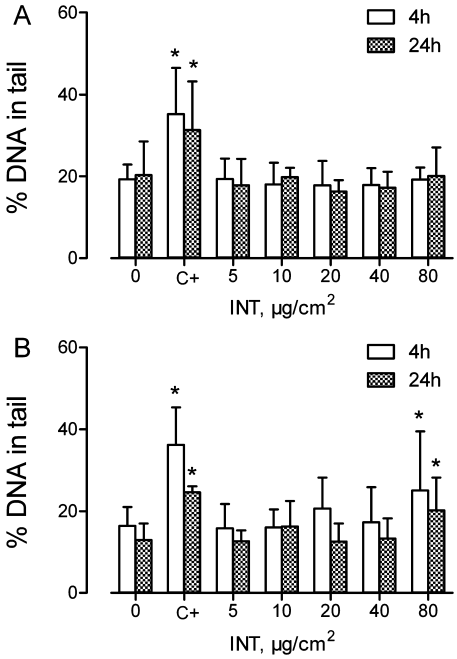

Figure 8. DNA damage (percent DNA in tail) in RAW264.7 (a) and A549 (b) cells exposed to different INT doses for 4 and 24 h. Methylmethanesulfonate (MMS; 0.5 mM) was used as a positive control (C+). Data are the mean with the SD (n = 6). * $p < 0.05$ (multiple range test).

composition/length, and absence of contaminants might account for the different results exhibited in our study.

Besides reporting the low cytotoxic and genotoxic potential of INT, in the present study we also addressed the activating effects of INT on macrophages. Macrophages may react to nanomaterials by eliciting several distinct activation pathways that determine tolerance to the material or the ability to elicit inflammatory changes that are possibly followed by fibrotic alterations.[32,75−78] In both RAW264.7 and MH-S cells, INT do not induce *Arg1*, a typical marker of alternative macrophage activation,[65−68] which underlies repair and fibrosis. Moreover, in the same models, no induction of *Nos2*[69−71] was detected, indicating that INT do not promote the classical activation of macrophages, which is correlated to ROS production and tissue damage. The absence of *Nos2* induction is consistent with the lack of nitrite accumulation in the medium, an indicator of NO production, and with the absence of marked cytotoxic effects. On the other hand, INT do not interfere with LPS-induced *Nos2* expression and nitrite accumulation. However, a significant induction of *Il6* was observed only in RAW264.7 cells but not in MH-S cells, suggesting that this finding is due to specific features of the former cell line rather than to a response to INT shared by all macrophage cells. Thus, in conclusion, INT do not appear to be able to elicit definite changes typical of either classical or alternative macrophage activation, although it still may produce changes in gene expression depending on the particular cell type employed.

Airway epithelial cells are the first barrier that nanostructured materials have to cross to reach the lung interstitial tissues and to be transported thereafter to other districts of the organism. Interestingly, both fibrous silicates[79−81] and carbon nanotubes, either SWCNT or MWCNT,[48,64] have been reported to alter the barrier properties of airway Calu-3 epithelial cells *in vitro*. In contrast, after 7 days of treatment, INT do not cause a significant increase of monolayer permeability on the same biological model, pointing to the substantial preservation of the epithelial cell barrier. These data also indicate that INT do not exert a significant cytotoxicity on the epithelial cells; indeed, if only a minor portion of the epithelial cell population was damaged by INT, then TEER would be expected to fall abruptly. However, because the TEER values recorded in monolayers treated with INT or SWCNT were not significantly different (Figure 11a), it is possible that INT may also damage the monolayer barrier at a longer incubation time. In conclusion, as far as epithelial barrier damage is concerned, the toxicity rank obtained is INT ≪ SWCNT < MWCNT. It should be stressed, however, that all of these experiments were performed in the presence of 10% FBS at both the apical and baso-lateral compartments. A more physiological approach would have been to use air−liquid interface cultures or a saline solution in the apical compartment to reproduce the *in vivo* situation more closely.

The mild effects of INT on all of the cell models tested may be related both to the presence of bridged Al(OH)Al groups at the INT surface and to their high hydrophilicity. It has been known since the beginning of the last century that aluminum ions are able to reduce the toxicity of crystalline silica.[82] The impregnation of quartz powders with an aluminum salt inhibits most adverse reactions to silica *in vivo* and decreases the generation of ROS and DNA damage caused by silica.[83,84] The mechanism of action of aluminum is poorly understood; however, it appears to affect the surface acidity, reducing the zeta potential. The external layer of aluminum is also responsible for the positive surface charge of INT observed in a large range of pH values.

Moreover, the abundance of OH groups renders the structure very hydrophilic.[85] The presence of water strongly adsorbed at the surface is evidenced by the high heat of adsorption and is confirmed by a previous study on the catalytic behavior of imogolite along with its thermal stability.[9] This study showed that the water inside nanotubes is completely desorbed only at 300 °C, whereas a temperature of 150 °C is sufficient to dehydrate amorphous silica. This strongly adsorbed water hinders molecular diffusion inside the narrow micropores.[9] Diffusion of molecules is also prevented because of the length of nanotubes, which can reach several micrometers. Moreover, silanols, which have been identified as the surface functionalities responsible for silica-related cell membrane damage,[86] are all exposed in the inside of the INT and hence are not available to the cells.

Table 2. Viability of RAW264.7 Cells

	cell viability (%)[a]						
imogolite (μg/cm^2)	0	C+	5	10	20	40	80
4 h	100 ± 0.0	83 ± 26.1	95 ± 5.7	96 ± 7,2	94 ± 3.6	84 ± 16.8	88 ± 8.5
24 h	95 ± 8.4	90 ± 8.6	100 ± 0.0	95 ± 10.0	100 ± 0.2	99 ± 0.9	96 ± 4.5

[a]Values are the mean ± SD. C+ = methylmethanesulfonate (0.5 mM).

dx.doi.org/10.1021/tx500002d | *Chem. Res. Toxicol.* 2014, 27, 1142−1154

Table 3. Viability of A549 Cells

	cell viability (%)[a]						
imogolite (μg/cm^2)	0	C+	5	10	20	40	80
4 h	97 ± 3.2	98 ± 2.4	95 ± 5.6	94 ± 1.9	93 ± 1.3	93 ± 3.5	91 ± 4.8[b]
24 h	95 ± 5.5	91 ± 0.1	94 ± 0.2	89 ± 4.8	92 ± 4.1	86 ± 5.0[b]	88 ± 6.8[b]

[a]Values are the mean ± SD. C+ = methylmethanesulfonate (0.5 mM). [b]$p < 0.05$ vs untreated cells.

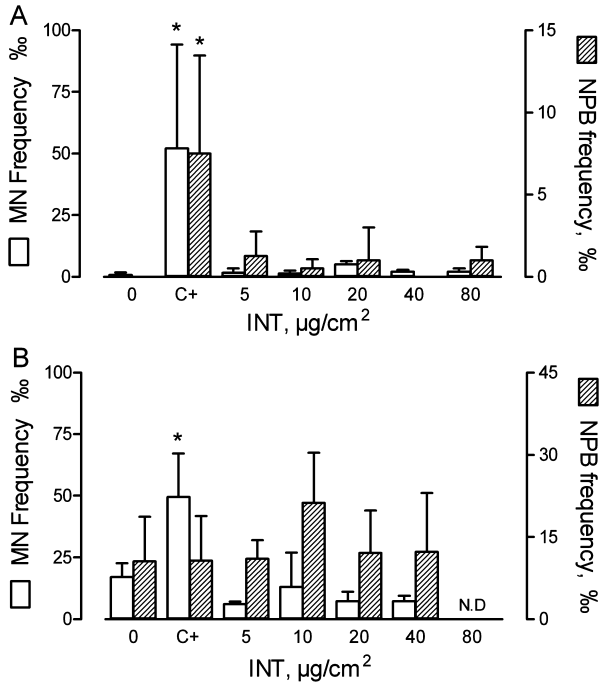

Figure 9. Frequency of micronuclei and nucleoplasmic bridges (NPB) in RAW264.7 (a) and A549 (b) cells after exposure to different INT doses. Mitomycin C was used as a positive control (C+). Data are the mean with the SD ($n = 4$). * $p < 0.05$ (multiple range test). N.D.: not enough cells to perform cytogenetic analyses.

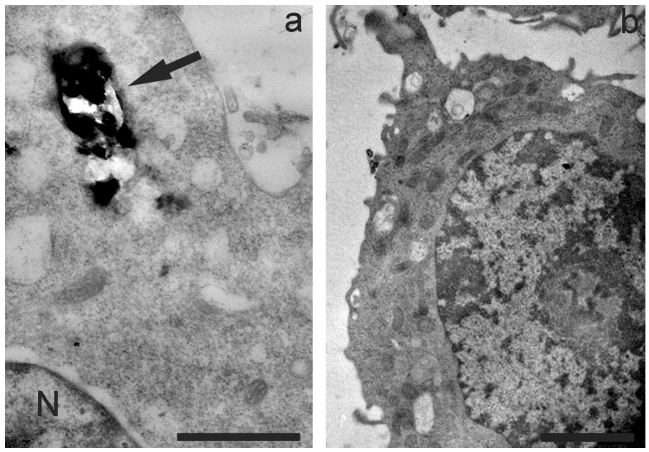

Figure 10. Transmission electron micrographs of RAW264.7 cells. Cells were incubated in the absence or presence of 80 μg/cm^2 INT for 24 h. (a) Exposed cell showing a densely packed imogolite inclusion (arrow). (b) Control cell devoid of dense inclusions. N = nucleus; scale bar = 1 μm for panel a and 2 μm for panel b.

In conclusion, although the morphology of INT suggests a potential toxicity, on the basis of their high length-to-diameter ratio and expected durability, all of the data reported point to mild, if any, toxic responses in a variety of cell models and tests

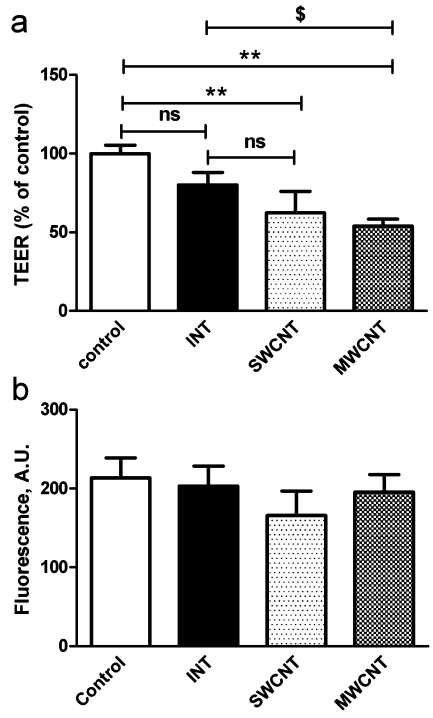

Figure 11. Differential effects of INT, SWCNT, and MWCNT on the trans-epithelial electrical resistance (TEER) and viability of Calu-3 monolayers. Calu-3 cells were cultured for 10 days on 0.4 μm membrane filters. At the end of this period, INT, SWCNT, or MWCNT, all at 80 μg/cm^2, were added to the apical chamber of the culture system. TEER (a) and viability (b) were determined after 7 days. Empty bar, control monolayers maintained in the absence of nanomaterials. The figure shows a representative experiment performed three times with comparable results. Data are the mean with the SD ($n = 4$). ** $p < 0.01$ vs control, untreated cultures; $ $p < 0.05$ vs MWCNT-treated monolayers; ns, not significant.

upon exposure to this kind of material. The extreme hydrophilicity and the presence of an external alumina layer in the absence of free radical release may contribute to the relative inertness of the material and support the feasibility of possible applications of INT in nanomedicine.

AUTHOR INFORMATION

Corresponding Authors

*(B.F.) Tel.: +39 011 6707566. Fax: +39 011 6707855. E-mail: bice.fubini@unito.it.

*(O.B.) Tel.: +39 0521 033783. Fax: +39 0521 033742. E-mail: ovidio.bussolati@unipr.it.

Author Contributions

[∇]B.M.R., P.G., and B.B. contributed equally to this work.

Funding

This work was supported by the Italian Ministry of University and Scientific-Technological Research (PRIN 2007498XRF, Study of the mechanisms responsible for cytotoxicity and

genotoxicity of silica nanoparticles and nanometric fibrous silicates having strictly controlled size, structure, and composition (national coordinator, Prof. Dario Ghigo); grant nos. 2007498XRF_002, "Effects of silica nanoparticles and silicate nanofibers on lung-blood barrier cells", to O.B. and 2007498XRF_003, "Mechanisms responsible for cytotoxicity and genotoxicity of silica nanoparticles and nanometric fibrous silicates having strictly controlled size, structure, and composition", to G.F).

Notes

The authors declare no competing financial interest.

■ ACKNOWLEDGMENTS

The authors are thankful to Claudio Ghezzani for his technical assistance in image analysis. This work is part of the Ph.D. thesis of P.G.

■ ABBREVIATIONS

BET, Brunauer–Emmett–Teller; BSA, bovine serum albumin; CBMN, cytokinesis-block micronucleus cytome; FBS, fetal bovine serum; FE-SEM, field emission scanning electron microscope; HARN, high-aspect ratio nanomaterials; IEP, isoelectric point; INT, imogolite nanotubes; LPS, lipopolysaccharide; MN, micronuclei; MWCNT, multiwalled carbon nanotubes; NL-DFT, nonlocal density functional theory; NOAEL, no observed adverse effect level; NPB, nucleoplasmic bridges; PSD, pore size distribution; SSA, specific surface area; SWCNT, single-walled carbon nanotubes; TEER, trans-epithelial electrical resistance

■ REFERENCES

(1) Kagan, V. E., Bayir, H., and Shvedova, A. A. (2005) Nanomedicine and nanotoxicology: two sides of the same coin. *Nanomedicine 1*, 313–316.

(2) Donaldson, K., Borm, P. J., Castranova, V., and Gulumian, M. (2009) The limits of testing particle-mediated oxidative stress *in vitro* in predicting diverse pathologies; relevance for testing of nanoparticles. *Part. Fibre Toxicol. 6*, 13.

(3) Xia, T., Li, N., and Nel, A. E. (2009) Potential health impact of nanoparticles. *Annu. Rev. Public Health 30*, 137–150.

(4) Oberdorster, G. (2010) Safety assessment for nanotechnology and nanomedicine: concepts of nanotoxicology. *J. Int. Med. 267*, 89–105.

(5) Donaldson, K., Murphy, F. A., Duffin, R., and Poland, C. A. (2010) Asbestos, carbon nanotubes and the pleural mesothelium: a review of the hypothesis regarding the role of long fibre retention in the parietal pleura, inflammation and mesothelioma. *Part. Fibre Toxicol. 7*, 5.

(6) Fubini, B., Fenoglio, I., Tomatis, M., and Turci, F. (2011) Effect of chemical composition and state of the surface on the toxic response to high aspect ratio nanomaterials. *Nanomedicine (London, U.K.) 6*, 899–920.

(7) Donaldson, K., Murphy, F., Schinwald, A., Duffin, R., and Poland, C. A. (2011) Identifying the pulmonary hazard of high aspect ratio nanoparticles to enable their safety-by-design. *Nanomedicine (London, U.K.) 6*, 143–156.

(8) Farmer, V. C. (1986) Sources and speciation of aluminium and silicon in natural waters. *Ciba Found. Symp. 121*, 4–23.

(9) Bonelli, B., Bottero, I., Ballarini, N., Passeri, S., Cavani, F., and Garrone, E. (2009) IR spectroscopic and catalytic characterization of the acidity of imogolite-based systems. *J. Catal. 264*, 15–30.

(10) Cradwick, P. D. G., Farmer, V. C., Russell, J. D., Masson, C. R., Wada, K., and Yoshinaga, N. (1972) Imogolite, a hydrated silicate of tubular nature. *Nature (London), Phys. Sci. 240*, 187–189.

(11) Bonelli, B., Armandi, M., and Garrone, E. (2013) Surface properties of alumino-silicate single-walled nanotubes of the imogolite type. *Phys. Chem. Chem. Phys. 15*, 13381–13390.

(12) Guimaraes, L., Pinto, Y. N., Lourenco, M. P., and Duarte, H. A. (2013) Imogolite-like nanotubes: structure, stability, electronic and mechanical properties of the phosphorous and arsenic derivatives. *Phys. Chem. Chem. Phys. 15*, 4303–4309.

(13) Gustafsson, J. P. (2001) The surface chemistry of imogolite. *Clays Clay Miner. 49*, 73–80.

(14) Bottero, I., Bonelli, B., Ashbrook, S. E., Wright, P. A., Zhou, W. Z., Tagliabue, M., Armandi, M., and Garrone, E. (2011) Synthesis and characterization of hybrid organic/inorganic nanotubes of the imogolite type and their behaviour towards methane adsorption. *Phys. Chem. Chem. Phys. 13*, 744–750.

(15) Pohl, P. I., Faulon, J. L., and Smith, D. M. (1996) Pore structure of imogolite computer models. *Langmuir 12*, 4463–4468.

(16) Ackerman, W. C., Smith, D. M., Huling, J. C., Kim, Y. W., Bailey, J. K., and Brinker, C. J. (1993) Gas/vapor adsorption in imogolite: a microporous tubular aluminosilicate. *Langmuir 9*, 1051–1057.

(17) Clark, C. J., and McBride, M. B. (1984) Cation and anion retention by natural and synthetic allophane and imogolite. *Clays Clay Miner. 32*, 291–299.

(18) Denaix, L., Lamy, I., and Bottero, J. Y. (1999) Structure and affinity towards Cd^{2+}, Cu^{2+}, Pb^{2+} of synthetic colloidal amorphous aluminosilicates and their precursors. *Colloids Surf., A 158*, 315–325.

(19) Imamura, S., Kokubu, T., Yamashita, T., Okamoto, Y., Kajiwara, K., and Kanai, H. (1996) Shape-selective copper-loaded imogolite catalyst. *J. Catal. 160*, 137–139.

(20) Levard, C., Rose, J., Masion, A., Doelsch, E., Borschneck, D., Olivi, L., Dominici, C., Grauby, O., Woicik, J. C., and Bottero, J. Y. (2008) Synthesis of large quantities of single-walled aluminogermanate nanotube. *J. Am. Chem. Soc. 130*, 5862–5863.

(21) Levard, C., Masion, A., Rose, J., Doelsch, E., Borschneck, D., Olivi, L., Chaurand, P., Dominici, C., Ziarelli, F., Thill, A., Maillet, P., and Bottero, J. Y. (2011) Synthesis of Ge-imogolite: influence of the hydrolysis ratio on the structure of the nanotubes. *Phys. Chem. Chem. Phys. 13*, 14516–14522.

(22) Levard, C., Masion, A., Rose, J., Doelsch, E., Borschneck, D., Dominici, C., Ziarelli, F., and Bottero, J. Y. (2009) Synthesis of imogolite fibers from decimolar concentration at low temperature and ambient pressure: a promising route for inexpensive nanotubes. *J. Am. Chem. Soc. 131*, 17080–17081.

(23) Maillet, P., Levard, C., Spalla, O., Masion, A., Rose, J., and Thill, A. (2011) Growth kinetic of single and double-walled aluminogermanate imogolite-like nanotubes: an experimental and modeling approach. *Phys. Chem. Chem. Phys. 13*, 2682–2689.

(24) Maillet, P., Levard, C., Larquet, E., Mariet, C., Spalla, O., Menguy, N., Masion, A., Doelsch, E., Rose, J., and Thill, A. (2010) Evidence of double-walled Al-Ge imogolite-like nanotubes. A cryo-TEM and SAXS investigation. *J. Am. Chem. Soc. 132*, 1208–1209.

(25) Liu, W., Chaurand, P., Di Giorgio, C., De Meo, M., Thill, A., Auffan, M., Masion, A., Borschneck, D., Chaspoul, F., Gallice, P., Botta, A., Bottero, J. Y., and Rose, J. (2012) Influence of the length of imogolite-like nanotubes on their cytotoxicity and genotoxicity toward human dermal cells. *Chem. Res. Toxicol. 25*, 2513–2522.

(26) Ishikawa, K., Akasaka, T., Yawaka, Y., and Watari, F. (2010) High functional expression of osteoblasts on imogolite, aluminosilicate nanotubes. *J. Biomed. Nanotechnol. 6*, 59–65.

(27) Farmer, V. C., Adams, M. J., Fraser, A. R., and Palmeri, F. (1983) Synthetic imogolite: properties, synthesis, and possible applications. *Clay Miner. 18*, 459–472.

(28) Landers, J., Gor, G. Y., and Neimark, A. V. (2013) Density functional theory methods for characterization of porous materials. *Colloids Surf., A 437*, 3–32.

(29) Ohshima, H. (1996) Henry's function for electrophoresis of a cylindrical colloidal particle. *J. Colloid Interface Sci. 180*, 299–301.

(30) Fubini, B., Mollo, L., and Giamello, E. (1995) Free radical generation at the solid/liquid interface in iron containing minerals. *Free Radical Res. 23*, 593–614.

(31) Mbawuike, I. N., and Herscowitz, H. B. (1989) Mh-S, a murine alveolar macrophage cell-line: morphological, cytochemical, and functional-characteristics. *J. Leukocyte Biol. 46*, 119–127.

(32) Xia, T., Kovochich, M., Brant, J., Hotze, M., Sempf, J., Oberley, T., Sioutas, C., Yeh, J. I., Wiesner, M. R., and Nel, A. E. (2006) Comparison of the abilities of ambient and manufactured nanoparticles to induce cellular toxicity according to an oxidative stress paradigm. *Nano Lett. 6*, 1794−1807.
(33) Thibodeau, M., Giardina, C., and Hubbard, A. K. (2003) Silica-induced caspase activation in mouse alveolar macrophages is dependent upon mitochondrial integrity and aspartic proteolysis. *Toxicol. Sci. 76*, 91−101.
(34) Soto, K., Garza, K. M., and Murr, L. E. (2007) Cytotoxic effects of aggregated nanomaterials. *Acta Biomater. 3*, 351−358.
(35) Scheel, J., Weimans, S., Thiemann, A., Heisler, E., and Hermann, M. (2009) Exposure of the murine RAW 264.7 macrophage cell line to hydroxyapatite dispersions of various composition and morphology: assessment of cytotoxicity, activation and stress response. *Toxicol. In Vitro 23*, 531−538.
(36) Ghiazza, M., Polimeni, M., Fenoglio, I., Gazzano, E., Ghigo, D., and Fubini, B. (2010) Does vitreous silica contradict the toxicity of the crystalline silica paradigm? *Chem. Res. Toxicol. 23*, 620−629.
(37) Gonzalez, L., Thomassen, L. C., Plas, G., Rabolli, V., Napierska, D., Decordier, I., Roelants, M., Hoet, P. H., Kirschhock, C. E., Martens, J. A., Lison, D., and Kirsch-Volders, M. (2010) Exploring the aneugenic and clastogenic potential in the nanosize range: A549 human lung carcinoma cells and amorphous monodisperse silica nanoparticles as models. *Nanotoxicology 4*, 382−395.
(38) Guidi, P., Nigro, M., Bernardeschi, M., Scarcelli, V., Lucchesi, P., Onida, B., Mortera, R., and Frenzilli, G. (2013) Genotoxicity of amorphous silica particles with different structure and dimension in human and murine cell lines. *Mutagenesis 28*, 171−180.
(39) Finkbeiner, W. E., Carrier, S. D., and Teresi, C. E. (1993) Reverse transcription-polymerase chain-reaction (RT-PCR) phenotypic analysis of cell-cultures of human tracheal epithelium, tracheobronchial glands, and lung carcinomas. *Am. J. Respir. Cell Mol. Biol. 9*, 547−556.
(40) Grainger, C. I., Greenwell, L. L., Martin, G. P., and Forbes, B. (2009) The permeability of large molecular weight solutes following particle delivery to air-interfaced cells that model the respiratory mucosa. *Eur. J. Pharm. Biopharm. 71*, 318−324.
(41) Togami, K., Chono, S., Seki, T., and Morimoto, K. (2009) Distribution characteristics of telithromycin, a novel ketolide antimicrobial agent applied for treatment of respiratory infection, in lung epithelial lining fluid and alveolar macrophages. *Drug Metab. Pharmacokinet. 24*, 411−417.
(42) Slutter, B., Bal, S. M., Que, I., Kaijzel, E., Lowik, C., Bouwstra, J., and Jiskoot, W. (2010) Antigen−adjuvant nanoconjugates for nasal vaccination: an improvement over the use of nanoparticles? *Mol. Pharmaceutics 7*, 2207−2215.
(43) Brillault, J., De Castro, W. V., and Couet, W. (2010) Relative contributions of active mediated transport and passive diffusion of fluoroquinolones with various lipophilicities in a Calu-3 lung epithelial cell model. *Antimicrob. Agents Chemother. 54*, 543−545.
(44) Bharatwaj, B., Wu, L. B., Whittum-Hudson, J. A., and da Rocha, S. R. P. (2010) The potential for the noninvasive delivery of polymeric nanocarriers using propellant-based inhalers in the treatment of Chlamydial respiratory infections. *Biomaterials 31*, 7376−7385.
(45) Bur, M., Huwer, H., Muys, L., and Lehr, C. M. (2010) Drug transport across pulmonary epithelial cell monolayers: effects of particle size, apical liquid volume, and deposition technique. *J. Aerosol Med. Pulm. Drug Delivery 23*, 119−127.
(46) Burgess, B. L., Cavigiolio, G., Fannucchi, M. V., Illek, B., Forte, T. M., and Oda, M. N. (2010) A phospholipid-apolipoprotein A-I nanoparticle containing amphotericin B as a drug delivery platform with cell membrane protective properties. *Int. J. Pharm. 399*, 148−155.
(47) O'Brien, J., Wilson, I., Orton, T., and Pognan, F. (2000) Investigation of the Alamar Blue (resazurin) fluorescent dye for the assessment of mammalian cell cytotoxicity. *Eur. J. Biochem. 267*, 5421−5426.
(48) Rotoli, B. M., Bussolati, O., Bianchi, M. G., Barilli, A., Balasubramanian, C., Bellucci, S., and Bergamaschi, E. (2008) Non-functionalized multi-walled carbon nanotubes alter the paracellular permeability of human airway epithelial cells. *Toxicol. Lett. 178*, 95−102.
(49) Bianchi, M. G., Gazzola, G. C., Tognazzi, L., and Bussolati, O. (2008) C6 glioma cells differentiated by retinoic acid overexpress the glutamate transporter excitatory amino acid carrier 1 (EAAC1). *Neuroscience 151*, 1042−1052.
(50) Visigalli, R., Barilli, A., Bussolati, O., Sala, R., Gazzola, G. C., Parolari, A., Tremoli, E., Simon, A., Closs, E. I., and Dall'Asta, V. (2007) Rapamycin stimulates arginine influx through CAT2 transporters in human endothelial cells. *Biochim. Biophys. Acta, Biomembr. 1768*, 1479−1487.
(51) Singh, N. P., McCoy, M. T., Tice, R. R., and Schneider, E. L. (1988) A simple technique for quantitation of low levels of DNA damage in individual cells. *Exp. Cell Res. 175*, 184−191.
(52) Fenech, M., Chang, W. P., Kirsch-Volders, M., Holland, N., Bonassi, S., and Zeiger, E. (2003) HUMN project: detailed description of the scoring criteria for the cytokinesis-block micronucleus assay using isolated human lymphocyte cultures. *Mutat. Res. 534*, 65−75.
(53) Fenech, M. (2007) Cytokinesis-block micronucleus cytome assay. *Nat. Protoc. 2*, 1084−1104.
(54) Salem, L. B., Bosquillon, C., Dailey, L. A., Delattre, L., Martin, G. P., Evrard, B., and Forbes, B. (2009) Sparing methylation of beta-cyclodextrin mitigates cytotoxicity and permeability induction in respiratory epithelial cell layers *in vitro*. *J. Controlled Release 136*, 110−116.
(55) Mollenhauer, H. H. (1964) Plastic embedding mixtures for use in electron microscopy. *Stain Technol. 39*, 111−114.
(56) Singh, B. P., Menchavez, R., Takai, C., Fuji, M., and Takahashi, M. (2005) Stability of dispersions of colloidal alumina particles in aqueous suspensions. *J. Colloid Interface Sci. 291*, 181−186.
(57) Arai, Y., McBeath, M., Bargar, J. R., Joye, J., and Davis, J. A. (2006) Uranyl adsorption and surface speciation at the imogolite-water interface: self-consistent spectroscopic and surface complexation models. *Geochim. Cosmochim. Acta 70*, 2492−2509.
(58) Park, S., Lee, Y., Kim, B., Lee, J., Jeong, Y., Noh, J., Takahara, A., and Sohn, D. (2007) Two-dimensional alignment of imogolite on a solid surface. *Chem. Commun.*, 2917−2919.
(59) Rezwan, K., Meier, L. P., Rezwan, M., Voros, J., Textor, M., and Gauckler, L. J. (2004) Bovine serum albumin adsorption onto colloidal Al_2O_3 particles: a new model based on zeta potential and UV−vis measurements. *Langmuir 20*, 10055−10061.
(60) Fenoglio, I., Greco, G., Tomatis, M., Muller, J., Raymundo-Pinero, E., Beguin, F., Fonseca, A., Nagy, J. B., Lison, D., and Fubini, B. (2008) Structural defects play a major role in the acute lung toxicity of multiwall carbon nanotubes: physicochemical aspects. *Chem. Res. Toxicol. 21*, 1690−1697.
(61) Gazzano, E., Ghiazza, M., Polimeni, M., Bolis, V., Fenoglio, I., Attanasio, A., Mazzucco, G., Fubini, B., and Ghigo, D. (2012) Physicochemical determinants in the cellular responses to nano-structured amorphous silicas. *Toxicol. Sci. 128*, 158−170.
(62) Fubini, B., Della Gatta, G., and Venturello, G. (1978) Energetics of adsorption in the alumina water system. Microcalorimetric study on the influence of adsorption temperature on surface processes. *J. Colloid Interface Sci. 64*, 470−479.
(63) Fubini, B., and Hubbard, A. (2003) Reactive oxygen species (ROS) and reactive nitrogen species (RNS) generation by silica in inflammation and fibrosis. *Free Radical Biol. Med. 34*, 1507−1516.
(64) Rotoli, B. M., Bussolati, O., Barilli, A., Zanello, P. P., Bianchi, M. G., Magrini, A., Pietroiusti, A., Bergamaschi, A., and Bergamaschi, E. (2009) Airway barrier dysfunction induced by exposure to carbon nanotubes in vitro: which role for fiber length? *Hum. Exp. Toxicol. 28*, 361−368.
(65) Louis, C. A., Mody, V., Henry, W. L., Reichner, J. S., and Albina, J. E. (1999) Regulation of arginase isoforms I and II by IL-4 in cultured murine peritoneal macrophages. *Am. J. Physiol.: Regul., Integr. Comp. Physiol. 276*, R237−R242.
(66) Morris, S. M., Kepka-Lenhart, D., and Chen, L. C. (1998) Differential regulation of arginases and inducible nitric oxide synthase in

murine macrophage cells. *Am. J. Physiol.: Endocrinol. Metab. 275*, E740−E747.
(67) Stempin, C., Giordanengo, L., Gea, S., and Cerban, F. (2002) Alternative activation and increase of *Trypanosoma cruzi* survival in murine macrophages stimulated by cruzipain, a parasite antigen. *J. Leukocyte Biol. 72*, 727−734.
(68) Raes, G., Van den Bergh, R., De Baetselier, P., Ghassabeh, G. H., Scotton, C., Locati, M., Mantovani, A., and Sozzani, S. (2005) Arginase-1 and Ym1 are markers for murine, but not human, alternatively activated myeloid cells. *J. Immunol. 174*, 6561.
(69) Yamashita, M., Niki, H., Yamada, M., Mue, S., and Ohuchi, K. (1997) Induction of nitric oxide synthase by lipopolysaccharide and its inhibition by auranofin in RAW 264.7 cells. *Eur. J. Pharmacol. 338*, 151−158.
(70) Munder, M., Eichmann, K., Moran, J. M., Centeno, F., Soler, G., and Modolell, M. (1999) Th1/Th2-regulated expression of arginase isoforms in murine macrophages and dendritic cells. *J. Immunol. 163*, 3771−3777.
(71) Chakravortty, D., Kato, Y., Sugiyama, T., Koide, N., Mu, M. M., Yoshida, T., and Yokochi, T. (2001) The inhibitory action of sodium arsenite on lipopolysaccharide-induced nitric oxide production in RAW 267.4 macrophage cells: a role of Raf-1 in lipopolysaccharide signaling. *J. Immunol. 166*, 2011−2017.
(72) White, K. N., Ejim, A. I., Walton, R. C., Brown, A. P., Jugdaohsingh, R., Powell, J. J., and McCrohan, C. R. (2008) Avoidance of aluminum toxicity in freshwater snails involves intracellular silicon-aluminum biointeraction. *Environ. Sci. Technol. 42*, 2189−2194.
(73) Jugdaohsingh, R., Brown, A., Dietzel, M., and Powell, J. J. (2013) High-aluminum-affinity silica is a nanoparticle that seeds secondary aluminosilicate formation. *PLoS One 8*, e84397.
(74) Muller, J., Huaux, F., Moreau, N., Misson, P., Heilier, J. F., Delos, M., Arras, M., Fonseca, A., Nagy, J. B., and Lison, D. (2005) Respiratory toxicity of multi-wall carbon nanotubes. *Toxicol. Appl. Pharmacol. 207*, 221−231.
(75) Bergamaschi, E., Bussolati, O., Magrini, A., Bottini, M., Migliore, L., Bellucci, S., Iavicoli, I., and Bergamaschi, A. (2006) Nanomaterials and lung toxicity: interactions with airways cells and relevance for occupational health risk assessment. *Int. J. Immunopathol. Pharmacol. 19*, 3−10.
(76) Sanchez, V. C., Pietruska, J. R., Miselis, N. R., Hurt, R. H., and Kane, A. B. (2009) Biopersistence and potential adverse health impacts of fibrous nanomaterials: what have we learned from asbestos? *Wiley Interdiscip. Rev.: Nanomed. Nanobiotechnol. 1*, 511−529.
(77) Shvedova, A. A., and Kagan, V. E. (2010) The role of nanotoxicology in realizing the 'helping without harm' paradigm of nanomedicine: lessons from studies of pulmonary effects of single-walled carbon nanotubes. *J. Int. Med. 267*, 106−118.
(78) Nagai, H., and Toyokuni, S. (2010) Biopersistent fiber-induced inflammation and carcinogenesis: lessons learned from asbestos toward safety of fibrous nanomaterials. *Arch. Biochem. Biophys. 502*, 1−7.
(79) Peterson, M. W., Walter, M. E., and Gross, T. J. (1993) Asbestos directly increases lung epithelial permeability. *Am. J. Physiol. 265*, L308−L317.
(80) Gardner, S. Y., Brody, A. R., Mangum, J. B., and Everitt, J. I. (1997) Chrysotile asbestos and H_2O_2 increase permeability of alveolar epithelium. *Exp. Lung Res. 23*, 1−16.
(81) Peterson, M. W., and Kirschbaum, J. (1998) Asbestos-induced lung epithelial permeability: potential role of nonoxidant pathways. *Am. J. Physiol.: Lung Cell. Mol. Physiol. 275*, L262−L268.
(82) Fubini, B. (1998) Health effects of silica, in *The Surface Properties of Silicas* (Legrand, A. P., Ed.) pp 415−464, J. Wiley and Sons, San Francisco, CA.
(83) Duffin, R., Gilmour, P. S., Schins, R. P. F., Clouter, A., Guy, K., Brown, D. M., MacNee, W., Borm, P. J., Donaldson, K., and Stone, V. (2001) Aluminium lactate treatment of DQ12 quartz inhibits its ability to cause inflammation, chemokine expression, and nuclear factor-kappa B activation. *Toxicol. Appl. Pharmacol. 176*, 10−17.
(84) Knaapen, A. M., Albrecht, C., Becker, A., Hohr, D., Winzer, A., Haenen, G. R., Borm, P. J. A., and Schins, R. P. F. (2002) DNA damage in lung epithelial cells isolated from rats exposed to quartz: role of surface reactivity and neutrophilic inflammation. *Carcinogenesis 23*, 1111−1120.
(85) Creton, B., Bougeard, D., Smirnov, K. S., Guilment, J., and Poncelet, O. (2008) Molecular dynamics study of hydrated imogolite. 2. Structure and dynamics of confined water. *Phys. Chem. Chem. Phys. 10*, 4879−4888.
(86) Slowing, I. I., Wu, C. W., Vivero-Escoto, J. L., and Lin, V. S. Y. (2009) Mesoporous silica nanoparticles for reducing hemolytic activity towards mammalian red blood cells. *Small 5*, 57−62.